NMR Study of Kinetic HH/HD/DH/DD Isotope Effects on the Tautomerism of Acetylporphyrin: Evidence for a Stepwise Double Proton Transfer

Martin Schlabach,[1a] Hans-Heinrich Limbach,*[1b] Edward Bunnenberg,[1c] Arthur Y. L. Shu,[1d] Bo-Ragnar Tolf,[1e] and Carl Djerassi*[1f]

Contribution from the Institut für Physikalische Chemie der Universität Freiburg i. Br. Albertstr. 21, D-7800 Freiburg, F.R.G., and Department of Chemistry, Stanford University, Stanford, California 94305

Received October 5, 1992

Abstract: The kinetic HH/HD/DH/DD isotope effects of an intramolecular reversible nondegenerate double proton transfer reaction are described. The molecule studied is 8-acetyl-3,13,17-tris[2-(methoxycarbonyl)ethyl]-2,7,12,18-tetramethyl-(21*H*,23*H*)-porphyrin (acetylporphyrin, ACP) dissolved in CD_2Cl_2. As a thermodynamic and kinetic method we used dynamic ^1H and ^{13}C NMR spectroscopy of suitably ^2H, ^{15}N, and ^{13}C labeled ACP. The ^{15}N label was introduced at the 21, 23, and 24 positions, the ^{13}C label at the 6- and 7-methyl positions, and ^2H at the central proton sites, respectively. The syntheses of these compounds are reported. ACP exists in two tautomeric forms of different energy which interconvert rapidly at room temperature and slowly at 200 K with respect to the NMR time scale. The tautomer with a proton located on the acetylpyrrole ring has the higher energy. The equilibrium constant for interconversion of the tautomers is given by $K = 1.14 \times \exp(-5.82 \text{ kJ mol}^{-1}/RT)$. Equilibrium isotope effects on the tautomerism of ACP are not observed within the margin of error. Whereas the tautomerism of ACP-HH and of ACP-DD can each be described by one rate constant, we find two different rate constants for ACP-HD: one for the HD and one for the DH reaction, respectively. In the HD reaction, an H atom jumps to the acetyl-substituted pyrrole ring; in the DH reaction, the D atom migrates. We obtain the following kinetic results: $k^{HH} = 10^{10.4} \exp(-40 \text{ kJ mol}^{-1}/RT)$, 230 K $\leq T \leq$ 327 K, $k^{HH}(298) \simeq 2840 \text{ s}^{-1}$, $k^{HD} = 10^{11.3} \exp(-52 \text{ kJ mol}^{-1}/RT)$, 266 K $\leq T \leq$ 311 K, $k^{HD}(298) \simeq 180 \text{ s}^{-1}$, $k^{DH} = 10^{10.0} \exp(-41 \text{ kJ mol}^{-1}/RT)$, 252 K $\leq T \leq$ 312 K, $k^{DH}(298) \simeq 670 \text{ s}^{-1}$, $k^{DD} = 10^{11.5} \exp(-53.5 \text{ kJ mol}^{-1}/RT)$, 273 K $\leq T \leq$ 380 K, $k^{DD}(298) \simeq 150 \text{ s}^{-1}$, with the kinetic isotope effects of $k^{HH}/k^{HD} \simeq 16$, $k^{HH}/k^{DH} \simeq 4$, $k^{HH}/k^{DD} \simeq 19$, $k^{HD}/k^{DD} \simeq 1.2$, $k^{DH}/k^{DD} \simeq 4.5$ at 298 K. These results are modeled in terms of a stepwise proton transfer. The HD and the DD reaction are characterized by similar rate constants because in both cases, a deuterium is transferred in the rate-determining step. The implications of these results to other chemically and biologically relevant multiple proton-transfer systems are discussed.

Information on the tautomerism of symmetrically substituted porphyrins, where two hydrogen atoms migrate between the four nitrogen atoms, has been obtained mainly by liquid[2-14] and solid state[14-20] dynamic NMR spectroscopy, as well as by optical spectroscopy.[21] In the discussion of the reaction pathways, the evaluation of the kinetic HH/DD[2,9,21] and the complete HH/HD/DD isotope effects[13,14] on the tautomerism has been of special importance. Initially, a concerted mechanism was proposed as shown in Figure 1, part a, involving proton tunneling at low temperatures.[9,13] However, further studies of kinetic HH/HD/DD isotope effects on degenerate double proton transfer reactions[22-26] confirmed a stepwise reaction pathway involving metastable cis-tautomers as shown in Figure 1, part b,[14] for which theoretical and experimental evidence had been previously obtained.[21,27-30]

(1) (a) Universität Freiburg, present address: Norwegian Institute for Air Research, P.O. Box 64, N-2001 Lillestrøm, Norway. (b) Universität Freiburg, present address: Institut für Organische Chemie der Freien Universität Berlin, Takustr.3, W-1000 Berlin 33. (c) Stanford University, decreased. (d) Stanford University, present address: Smith, Kline & French Laboratories, P.O. Box 7929, Swedeland, PA 10479. (e) Stanford University, present address: Astra Arcus AB, S-15185 Södertälje, Sweden. (f) Stanford University.

(2) Storm, C. B.; Teklu, Y. *J. Am. Chem. Soc.* **1972**, *94*, 1745. Storm, C. B.; Teklu, Y. *Ann. N. Y. Acad. Sci.* **1973**, *206*, 631.

(3) Abraham, R. J.; Hawkes, G. E.; Smith, K. M. *Tetrahedron Lett.* **1974**, 1483; Abraham, R. J.; Hawkes, G. E.; Smith, K. M. *J. Chem. Soc. Perkin Trans. 2* **1974**, 1483.

(4) Yeh, H. J. C.; Sato, M.; Morishima, I. *J. Magn. Reson.* **1977**, *26*, 365.

(5) Gust, D.; Roberts, J. D. *J. Am. Chem. Soc.* **1977**, *99*, 3637.

(6) Irving, C. S.; Lapidot, A. *J. Chem. Soc. Chem. Commun.* **1977**, 184.

(7) Eaton, S. S.; Eaton, G. R. *J. Am. Chem. Soc.* **1977**, *99*, 1601.

(8) Clezy, P. S.; Fookes, C. J. R.; Sternhell, S. *Aust. J. Chem.* **1978**, *31*, 639.

(9) Limbach, H.-H.; Hennig, J. *J. Chem. Soc. Faraday Trans. 2* **1979**, *75*, 752.

(10) Stilbs, P.; Moseley, M. E. *J. Chem. Soc. Faraday Trans. 2* **1980**, *76*, 729. Stilbs, P. *J. Magn. Reson.* **1984**, *58*, 152.

(11) Hennig, J.; Limbach, H. H. *J. Magn. Reson.* **1982**, *49*, 322.

(12) Hennig, J.; Limbach, H. H. *J. Am. Chem. Soc.* **1984**, *106*, 869.

(13) Limbach, H. H.; Hennig, J.; Gerritzen, D.; Rumpel, H. *Faraday Discuss. Chem. Soc.* **1982**, *74*, 822.

(14) Schlabach, M.; Wehrle, B.; Rumpel, H.; Braun, J.; Scherer, G.; Limbach, H. H. *Ber. Bunsenges. Phys. Chem.* **1992**, *96*, 821.

(15) Limbach, H. H.; Hennig, J.; Kendrick, R. D.; Yannoni, C. S. *J. Am. Chem. Soc.* **1984**, *106*, 4059.

(16) Wehrle, B.; Limbach, H. H.; Köcher, M.; Ermer, O.; Vogel, E. *Angew. Chem.* **1987**, *99*, 914.

(17) Limbach, H. H.; Wehrle, B.; Schlabach, M.; Kendrick, R. D.; Yannoni, C. S. *J. Magn. Reson.* **1988**, *77*, 84.

(18) Wehrle, B.; Limbach, H. H. *Chem. Phys.* **1989**, *136*, 223.

(19) Frydman, L.; Olivieri, A. C.; Diaz, L. E.; Frydman, B.; Morin, F. G.; Mayne, C. L.; Grant, D. M.; Adler, A. D. *J. Am. Chem. Soc.* **1988**, *110*, 336.

(20) Frydman, L.; Olivieri, A. C.; Diaz, L. E.; Valasinas, A.; Frydman, B. *J. Am. Chem. Soc.* **1988**, *110*, 5651.

(21) Butenhoff, T. B.; Moore, C. B. *J. Am. Chem. Soc.* **1988**, *110*, 8336.

(22) Limbach, H. H. Dynamic NMR Spectroscopy in the Presence of Kinetic Hydrogen/Deuterium Isotope Effects. *NMR Basic Principles and Progress*; Springer: Berlin, Heidelberg, New York, 1990; Vol. 26, Chapter 2.

(23) Rumpel, H.; Limbach, H. H. *J. Am. Chem. Soc.* **1989**, *111*, 5429; Rumpel, H.; Limbach, H. H.; Zachmann, G. *J. Phys. Chem.* **1989**, *93*, 1812.

(24) Scherer, G.; Limbach, H. H. *J. Am. Chem. Soc.* **1989**, *111*, 5946.

(25) Gerritzen, D.; Limbach, H. H. *J. Am. Chem. Soc.* **1984**, *106*, 869.

(26) Limbach, H. H.; Meschede, L.; Scherer, G. *Z Naturf.* **1989**, *44a*, 459. Meschede, L.; Limbach, H. H. *J. Phys. Chem.* **1991**, *95*, 10276.

(27) Kusmitzky, V. A.; Solovyov, K. N. *J. Mol. Struct.* **1980**, *65*, 219.

(28) Sarai, A. *J. Chem. Phys.* **1982**, *76*, 5554. Sarai, A. *J. Chem. Phys.* **1984**, *80*, 5431.

(29) Merz, K. M.; Reynolds, C. H. *J. Chem. Soc. Chem. Commun.* **1988**, 90.

(30) Smedarchina, Z.; Siebrand, W.; Wildman, T. A. *Chem. Phys. Lett.* **1988**, *143*, 395.

0002-7863/93/1515-4554$04.00/0

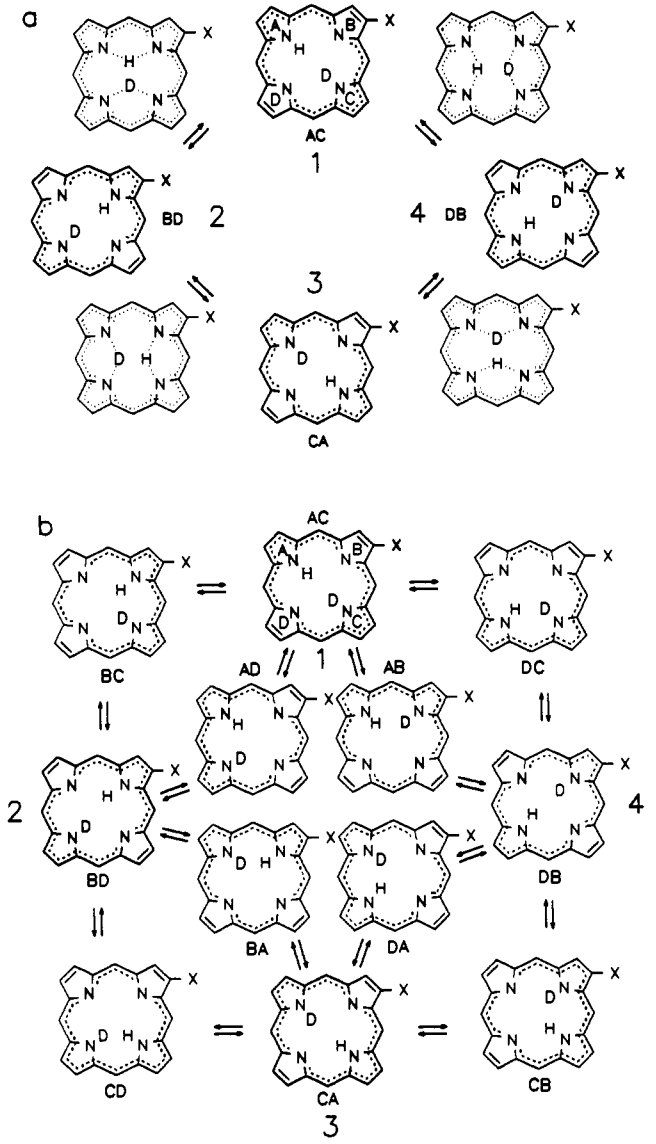

Figure 1. The tautomerism of asymmetrically substituted porphyrins. There may be additional substituents which are omitted for a better survey. Only the reaction is shown where one H and one D are transferred. (a) Hypothetical concerted reaction pathway. (b) Stepwise reaction pathway. As shown in the paper, the tautomers with a hydrogen isotope on ring B are less abundant than the other tautomers when X = acetyl. The reaction AC→BD→CA is faster than the reaction AC→DB→CA because in the latter, a deuteron has to jump to ring B.

Recent papers revealed that dynamic NMR spectroscopy is also capable of providing rate constants of the porphyrin tautomerism when the degeneracy of the porphyrin system is lifted either by solid state effects or by chemical substitution.[2,14,15,31-35] In this case, the reactions from tautomer AC to BD and from AC to DB may no longer be equivalent.[32,33] The problem of kinetic hydrogen/deuterium isotope effects is then

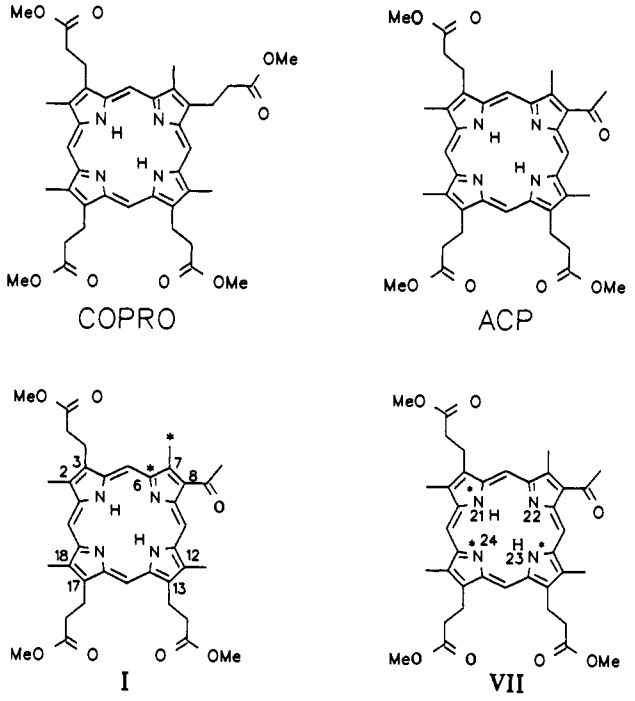

Figure 2. Structure of coproporphyrin-III tetramethylester (COPRO) and of the title compound 8-acetyl-3,13,17-tris[2-(methoxycarbonyl)ethyl]-2,7,12,18-tetramethyl-(21*H*,23*H*)-porphyrin (ACP). **I** is the ACP isotopomer labeled in this study doubly with ^{13}C, and **VII** is the isotopomer labeled triply with ^{15}N in the positions indicated by the asterisks.

more complex and has not yet been studied in detail. Asymmetrically substituted porphyrins are, therefore, interesting model systems for studying multiple kinetic hydrogen/deuterium isotope effects on nondegenerate double proton transfer reactions. The knowledge of these effects could be useful for the interpretation of organic or biochemical reactions.[36-39] The advantage of asymmetrically substituted porphyrins as model reactions lies in the fact that they represent reversible reaction sequences, whereas other sequences are often one-directional. In order to treat the problem of isotope effects on the tautomerism of asymmetrically substituted porphyrins, the theory of stepwise double proton transfer of Albery[37,38] was recently extended from the irreversible to the reversible case.[40] The theory was used to explain isotope effects on the tautomerism of 5,10,15,20-tetraphenylchlorin, where only the rate constants of the HH and the HD reaction but not of the DD reaction could be measured experimentally.[40]

In this report, we describe the results of a dynamic NMR study of multiple kinetic hydrogen/deuterium isotope effects on the tautomerism of 8-acetyl-3,13,17-tris[2-(methoxycarbonyl)-ethyl]-2,7,12,18-tetramethyl-(21*H*,23*H*)-porphyrin (ACP) dissolved in CD_2Cl_2. The structure of this compound is shown in Figure 2 where it is compared to the structure of coproporphyrin-III tetramethyl ester (COPRO). Whereas the tautomerism in COPRO is quasidegenerate within the margin of error of dynamic NMR spectroscopy,[6] the substitution with the acetyl group in ACP leads to a strong perturbation of the tautomerism. Evidence for a tautomerism of ACP was initially obtained by variable temperature magnetic circular dichroism (MCD) measurements[31] and was further corroborated by dynamic NMR experiments[34]

(31) Lu, Y.; Shu, A. Y.; Knierzinger, A.; Clezy, P.; Bunnenberg, E.; Djerassi, C. *Tetrahedron Lett.* **1983**, *24*, 2433. Djerassi, C.; Lu, Y.; Waleh, A.; Shu, A. Y.; Goldbeck, L. A. K.; Crandell, C. W.; Wee, A. G. H.; Knierzinger, A.; Gaete-Holmes, R.; Loew, G. H.; Clezy, P.; Bunnenberg, E. *J. Am. Chem. Soc.* **1984**, *106*, 4241.

(32) Crossley, M. J.; Harding, M. M.; Sternhell, S. *J. Am. Chem. Soc.* **1986**, *108*, 3608.

(33) Crossley, M. J.; Field, L. D.; Harding, M. M.; Sternhell, S. *J. Am. Chem. Soc.* **1987**, *109*, 2335. Crossley, M. J.; Harding, M. M.; Sternhell, S. *J. Org. Chem.* **1992**, *57*, 1833.

(34) Schlabach, M.; Wehrle, B.; Limbach, H. H.; Bunnenberg, E.; Knierzinger, A.; Shu, A. Y. L.; Tolf, B. R.; Djerassi, C. *J. Am. Chem. Soc.* **1986**, *108*, 3856.

(35) Schlabach, M.; Rumpel, H.; Limbach, H. H. *Angew. Chem.* **1989**, *101*, 84 and *Angew. Chem. Int. Ed. Engl.* **1989**, *28*, 78.

(36) Gandour, R. L.; Schowen, R. L. *Transition States of Biochemical Processes*; Plenum Press: New York, 1978.

(37) Albery, W. J. *Prog. React. Kinet.* **1967**, *4*, 355. Albery, W. J. *J. Phys. Chem.* **1986**, *90*, 3774.

(38) Belasco, J. G.; Albery, W. J.; Knowles, J. R. *Biochemistry* **1986**, *25*, 2529. *Ibid.* **1986**, *25*, 2552.

(39) Ahlberg, P.; Janné, K.; Löfås, S.; Nettelblad, F.; Swahn, L. *J. Phys. Org. Chem.* **1989**, *2*, 429.

(40) Schlabach, M.; Scherer, G.; Limbach, H.-H. *J. Am. Chem. Soc.* **1991**, *113*, 3550.

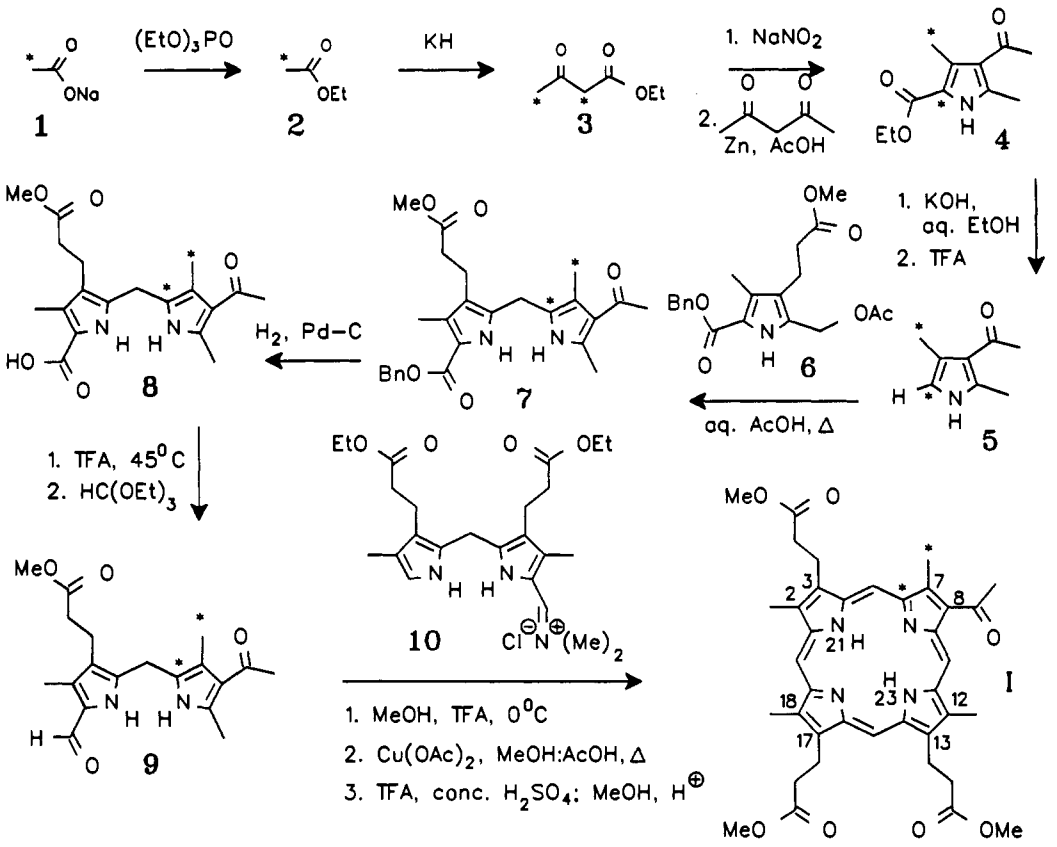

Figure 3. Synthesis of ^{13}C-labeled acetylporphyrin from sodium acetate. (*) ^{13}C-Labeled positions.

which revealed that this reaction is characterized by strong kinetic hydrogen/deuterium isotope effects. This study shows that the tautomerism of ACP can effectively be described in terms of the step AC→DB in Figure 1 which involves a complete set of multiple kinetic HH/HD/DH/DD isotope effects.

In order to resolve the different kinetic isotope effects it was necessary to synthesize various isotopically labeled ACP isotopomers. The syntheses of these compounds, which include the doubly ^{13}C-labeled and the triply ^{15}N-labeled isotopomers I and VII (Figure 2) are reported in the Experimental Section. The latter also contains the conditions of the NMR measurements and the theory used to simulate the exchange-broadened ^1H and ^{13}C NMR spectra of ACP. Subsequently, the results of the ^1H and ^{13}C NMR experiments are described and discussed.

Experimental Section

Synthesis of Isotopically Labeled ACP. In order to facilitate the discussion of the syntheses of doubly ^{13}C- and triply ^{15}N-labeled ACP, we use arabic numbers for the characterization of reagents and intermediates and Roman numbers for the ACP isotopomers.

Synthesis of ^{13}C-Labeled ACP. 8-Acetyl-3,13,17-tris[2-(methoxycarbonyl)ethyl]-2,7,12,18-(7-^{13}C)tetramethyl-(21*H*,23*H*)-(6-^{13}C)porphyrin (**I**) was synthesized according to literature procedures[41,42] modified here for the isotopically enriched material as shown in Figure 3. As a source for ^{13}C we used 90% enriched sodium (2-^{13}C)acetate **1** which leads to 8-acetyl-3,13,17-tris[2-(methoxycarbonyl)ethyl]-2,7,12,18-(7-^{13}C)tetramethyl-(21*H*,23*H*)-(6-^{13}C)porphyrin (**I**) as the major isotopic species. However, **I** is not the only species which is formed during the synthesis; this is not only because **1** was enriched only to 90% in the 2-position with ^{13}C but also because it was accidentally mixed with about 3–6% sodium (1-^{13}C)acetate. As shown below, this "accident" enabled us later to correctly assign the ^{13}C NMR spectra of ACP.

All possible isotopic ^{13}C-labeled ACP species and their sources are listed in Figure 4. Several of the additional species were observed by ^{13}C NMR spectroscopy as shown in Results.

(41) Chaudry, I. A.; Clezy, P. S.; Diakiv, V. *Aust. J. Chem.* **1977**, *30*, 879.
(42) Smith, K.; Langry, K. C. *J. Org. Chem.* **1983**, *48*, 500.

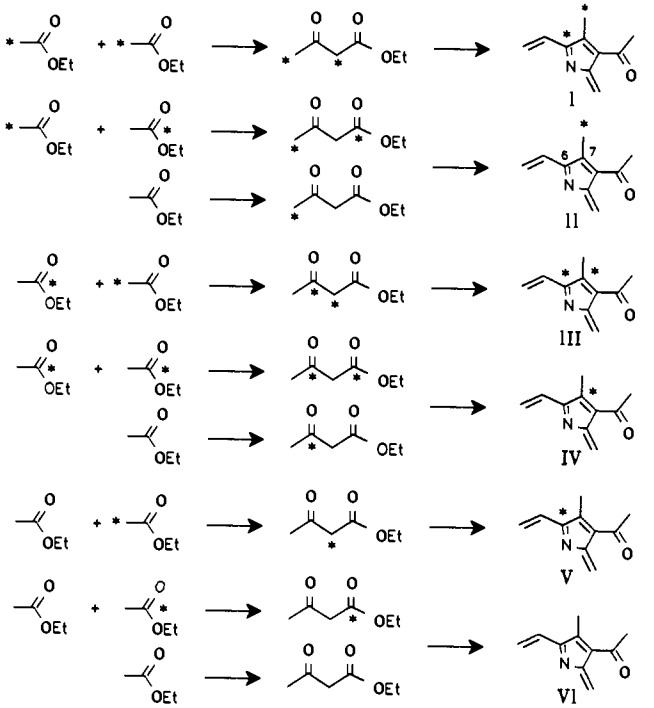

Figure 4. Isotope distribution in acetylporphyrin. (*) ^{13}C-Labeled positions.

Ethyl (2-^{13}C)Acetate (2). An amount of 3.58 g sodium (2-^{13}C)acetate (**1**) (90% ^{13}C, ICON Services, New Jersey, containing 3–6% sodium (1-^{13}C)acetate, 90% ^{13}C) was heated under reflux with freshly distilled triethyl phosphate (25 mL) to 180–200 °C for about 3 h. The product was degassed and purified by condensation[43] to yield 3.51 g (92%).

Ethyl (2,4-^{13}C)Acetoacetate (3). An excess amount of potassium hydride was washed five times with dry cyclohexane under an argon atmosphere in a previously weighed two-neck round-bottom flask. The

potassium hydride was dried and the excess gradually removed so that 0.82 g of dry potassium hydride remained. The powder was suspended in cyclohexane (20 mL) and heated to 50 °C under an argon atmosphere. Under vigorous stirring ethyl (2-^{13}C)acetate (**2**) (3.51 g) dissolved in cyclohexane (20 mL) was added dropwise and the temperature raised to 80 °C. After 3 h under reflux, the solvent was removed and the residue dissolved in 50% acetic acid and extracted with diethyl ether. The ether phase was washed with a bicarbonate solution and water and dried ($MgSO_4$). The ether was evaporated and the product distilled under reduced pressure. To avoid distillation losses, the receiver was cooled with liquid nitrogen. Yield: 0.622 g (~7% of the theoretical yield). We ascribe the small yield to losses during the distillation procedure.

Ethyl 4-Acetyl-3,5-(3-^{13}C)dimethyl-(2-^{13}C)pyrrole-2-carboxylate (4). Ethyl acetoacetate (**3**) (0.62 g) was nitrosated in acetic acid (2 mL) with $NaNO_2$ (0.36 g) dissolved in water (0.5 mL) at 5 °C. The yellow, viscous liquid was allowed to stand at ambient temperature overnight, then added dropwise (1 h) simultaneously with zinc dust (1.84 g) under stirring to 3,4-pentanedione (0.70 g) dissolved in acetic acid (5 mL) containing sodium acetate (1.5 g) at 50 °C. After the addition was completed, the mixture was refluxed gently for 0.5 h and thereafter allowed to reach room temperature. Water (20 mL) was added and the mixture extracted with CH_2Cl_2 (3 × 25 mL). The combined extracts were washed with saturated bicarbonate and water and then dried ($MgSO_4$). After evaporation, the residue was purified by column chromatography (silica gel) using ethyl acetate–hexane (1:1) as eluent thus affording 0.74 g (75%) of **4**.[44]

3-Acetyl-2,4-(4-^{13}C)dimethyl-(2-^{13}C)pyrrole (5). The preceding ester **4** (0.74 g) was suspended in a solution of KOH (0.5 g) in ethanol (15 mL) and water (1.5 mL). The mixture was heated to reflux for 3.5 h and then evaporated. Water (5 mL) was added to the residue and the resulting solution cooled in an ice–salt bath and acidified to pH 3–4 with 6 M HCl. The precipitate was filtered, washed with water, and dried in vacuo over $CaCl_2$ to yield 0.62 g (97%) of the corresponding acid. The above-mentioned acid (0.62 g), dissolved under nitrogen in trifluoroacetic acid (2.5 mL), was gently heated with a heat-gun for 10 min and was then immediately poured into an ice-cold solution of 4 M NH_4OH (35 mL). The mixture was extracted with chloroform (5 × 20 mL) and the organic layer washed with brine, dried (Na_2SO_4), and evaporated giving after drying in vacuo 0.46 g (96% from the acid) of **5**.[45,46]

Benzyl 4′-Acetyl-3-[2-(methoxycarbonyl)ethyl]-4,3′,5′-(3′-^{13}C)trimethyl-2,2′-(2′-^{13}C)dipyrrylmethane-5-carboxylate (7). The acetylpyrrole **5** (0.46 g) was dissolved in glacial acetic acid (15 mL) whereupon water (22 mL) and benzyl 5-(acetoxymethyl)-4-[2-(methoxycarbonyl)ethyl]-3-methylpyrrole-2-carboxylate (**6**) (1.28 g) were added. The resulting slurry was gradually heated (45 min) to 85 °C under nitrogen and then kept at the indicated temperature for 10 min at which time a reddish oil separated from the reaction mixture. Ice–water (15 mL) was added and the mixture extracted with CH_2Cl_2 (5 × 15 mL). The combined extracts were washed with saturated $NaHCO_3$ (3 × 30 mL) and water (50 mL) and then dried (Na_2SO_4). Evaporation and purification by column chromatography over silica gel using CH_2Cl_2–diethyl ether (95:5) as eluent gave 1.38 g (93%) of **7**.

4′-Acetyl-3-[2-(methoxycarbonyl)ethyl]-4,3′,5′-(3-^{13}C)trimethyl-2,2′-(2′-^{13}C)-dipyrrylmethane-5-carboxylic Acid (8). The benzyl ester **7** (1.37 g) was hydrogenated in a mixture of ethanol (30 mL) and THF (15 mL) over 10% Pd–C (0.14 g). When the reaction was completed, the mixture was evaporated and the residue dissolved in 4 M NH_4OH (40 mL) and filtered through Celite. The alkaline solution was cooled in an ice–salt bath and the product precipitated with 6 M HCl under nitrogen. Filtration under a stream of nitrogen and drying in vacuo over $CaCl_2$ afforded 1.02 g (93%) of the carboxylic acid **8**.[47]

4′-Acetyl-3-[2-(methoxycarbonyl)ethyl]-4,3′,5′-(3-^{13}C)trimethyl-2,2′-(2′-^{13}C)-dipyrrylmethane-5-carboxaldehyde (9). The above acid **8** (1.02 g) was dissolved under nitrogen in trifluoroacetic acid (5.0 mL) and immediately immersed into a preheated (45 °C) oil bath for 3 min. After being cooled in an ice bath for 4 min, triethyl orthoformate (1.50 mL) was added dropwise during 1 min and the mixture stirred for 10 min at 0 °C and then poured into ice–water (50 mL). The solid precipitate was collected and treated with a mixture of ethanol (8 mL) and 1 M NH_4OH (20 mL). The mixture was stirred for 20 min and then filtered. After drying and chromatography on neutral alumina III using CH_2Cl_2 as eluent, 778 mg (84%) of **9** was obtained.[47,48]

8-Acetyl-3,13,17-tris[2-(methoxycarbonyl)ethyl]-2,7,12,18-tetramethyl-(21*H*,23*H*)-(6-^{13}C)porphyrin (I). The aldehyde **9** (0.75 g) and the monoiminium salt **10**[49,50] were suspended in anhydrous methanol (15 mL) at 0 °C under nitrogen, and trifluoroacetic acid (4.2 mL) was added dropwise during 15 min in the dark. The reaction mixture was stirred at 0 °C for 2 h in the dark while *b*-bilene formation was followed spectrophotometrically by the appearance of an absorption band at λ_{max} = 504 nm. The mixture was thereafter poured into a refluxing solution of methanol (400 mL), glacial acetic acid (320 mL) containing copper(II) acetate (2.8 g), and anhydrous sodium acetate (2.8 g). The reaction was refluxed for 12 h in the dark and then diluted with water (800 mL). The aqueous mixture was repeatedly extracted with CH_2Cl_2, and the combined extracts washed with water and dried (Na_2SO_4). Evaporation and column chromatography of the residue over alumina III using CH_2Cl_2 as eluent afforded 325 mg of the copper(II) porphyrin, which was subsequently demetalized by treatment with trifluoroacetic acid (3 mL) and concd H_2SO_4 (10 mL) for 20 min, followed by careful addition to cold anhydrous methanol (250 mL) to allow reesterification. The methanol solution was kept in the dark overnight and then diluted with water (750 mL) and extracted with CH_2Cl_2. The combined extracts were washed with saturated $NaHCO_3$ and water and then dried (Na_2SO_4). The residue after evaporation was purified by column chromatography over silica gel using CH_2Cl_2/diethyl ether (95:5) as eluent to afford 112 mg (8%) of the title porphyrin after recrystallization from CH_2Cl_2–methanol.[49,50]

Synthesis of ($^{15}N_3$)Acetylporphyrin (VII). The triply ^{15}N-labeled acetylporphyrin **VII** was synthesized in an analogous way[41,42] as shown in Figure 5. For the synthesis, 99% enriched $Na^{15}NO_2$ was employed.

Benzyl 4-[2-(Methoxycarbonyl)ethyl]-3,5-dimethyl-(^{15}N)pyrrole-2-carboxylate (12). The standard Knorr procedure was used, except that the limiting reagent was $Na^{15}NO_2$. $Na^{15}NO_2$ (2.5 g) in water (5 mL) was added dropwise to a cold solution of benzyl acetoacetate (7 g) in glacial acetic acid. The mixture was further stirred at 0 °C for 2 h and at room temperature for another 2 h. The mixture was then added dropwise to a heated solution of 3-[(methoxycarbonyl)ethyl]-2,4-pentanedione (6.9 g) in glacial acetic acid (25 mL) with simultaneous addition of small portions of zinc dust (10 g) and anhydrous sodium acetate (10 g). The temperature of the reaction was kept below 90 °C. After completion of addition, the mixture was refluxed for 1 h and then poured into ice–water (500 mL). Collection through filtration and chromatography on silica gel with CH_2Cl_2/hexane (1:1) as eluent gave 8 g (70%) of the pyrrole.

Benzyl 5-(Acetoxymethyl)-4-[2-(methoxycarbonyl)ethyl]-3,5-dimethyl-(^{15}N)pyrrole-2-carboxylate (13). To a solution of **12** (2.2 g) in glacial acetic acid (20 mL) was added lead tetraacetate (3 g) in one portion. The reaction was stirred at room temperature under nitrogen for 4 h. Water (200 mL) was added and the precipitated solid was collected by filtration. Chromatography on silica gel column with CH_2Cl_2/hexane as eluent gave 2 g (75%) of **13**.

Dibenzyl 3,3′-Bis[2-(methoxycarbonyl)ethyl]-4,4′-dimethyl-2,2′-(1,1′-^{15}N)dipyrrylmethane-5,5′-dicarboxylate (15). The pyrrole **13** (5 g) was heated in a mixture of glacial acetic acid (35 mL) and water (9 mL) at 90 °C for 90 min under nitrogen. After cooling, 10% aqueous sodium acetate (150 mL) was added and the solid collected by filtration. Recrystallization from methanol gave 3.5 g (40%) of the dipyrrylmethane **15**.

Benzyl 4′-Acetyl-3-[2-(methoxycarbonyl)ethyl]-4,3′,5′-trimethyl-2,2′-(1-^{15}N)dipyrrylmethane-5-carboxylate (17). The labeled α-acetoxy pyrrole **13** (5 g) was heated with 3,5-dimethyl-4-acetylpyrrole (**14**) (2.1 g) in a mixture of glacial acetic acid (40 mL) and water (70 mL) at 90 °C for 1 h under nitrogen. Dilution with cold water, filtration, and recrystallization from chloroform–hexane gave 4.7 g (77%) of the dipyrrylmethane **17**.

4′-Acetyl-3-[2-(methoxycarbonyl)ethyl]-4,3′,5′-trimethyl-2,2′-(1-^{15}N)-dipyrrylmethane-5-carboxaldehyde (18). The dipyrrylmethane ester **17** (4.5 g) was hydrogenated as described for the ^{13}C analogue, affording 3.4 g (93%) of the corresponding acid. The acid was dissolved in trifluoroacetic acid (10 mL) and heated at 45 °C for 3 min. After cooling

(43) Ott, D. G. *Synthesis with Stable Isotopes*; John Wiley & Sons: New York, 1981.
(44) Fischer, H. *Org. Synth.* **1941**, *21*, 67.
(45) Howarth, T. T.; Jackson, A. H.; Judge, J.; Kenner, G. W.; Newman, D. J. *J. Chem. Soc., Perkin I* **1974**, 490.
(46) Clezy, P. S.; Liepa, A. J. *Aust. J. Chem.* **1970**, *23*, 2443.
(47) Clezy, P. S.; Liepa, A. J. *Aust. J. Chem.* **1970**, *23*, 2461.
(48) Clezy, P. S.; Fookes, C. J. R.; Liepa, A. J. *Aust. J. Chem.* **1972**, *25*, 1979.
(49) Clezy, P. S.; Liepa, A. J.; Webb, N. W. *Aust. J. Chem.* **1972**, *25*, 1991.
(50) Wee, A. G. H.; Shu, A. Y. L.; Bunnenberg, E.; Djerassi, C. *J. Org. Chem.* **1984**, *49*, 3327.

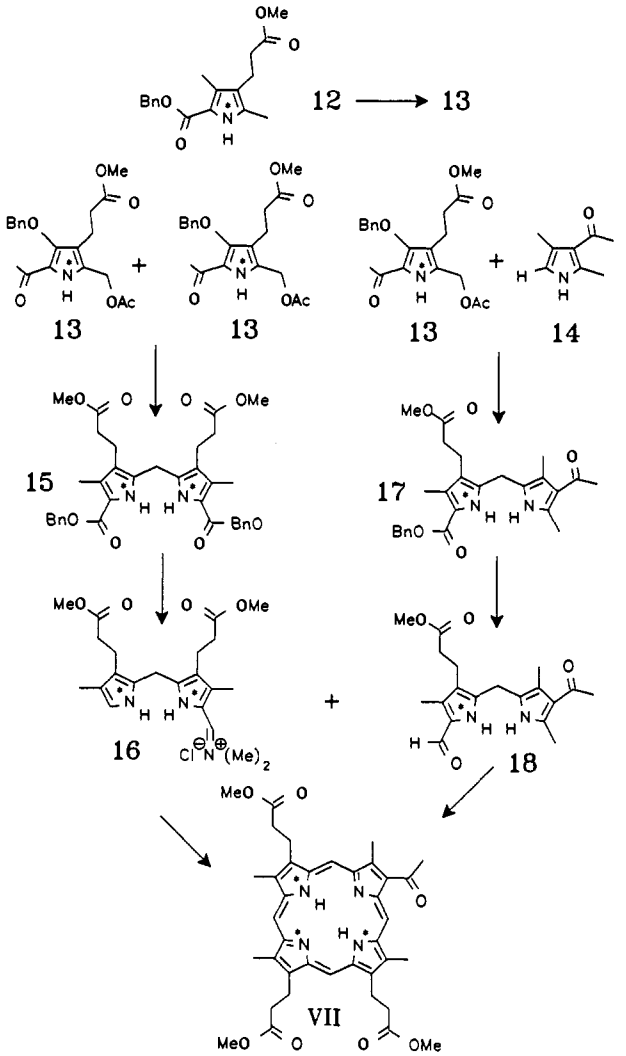

Figure 5. Synthesis of ^{15}N-labeled acetylporphyrin. (*) ^{15}N-Labeled positions.

to 0 °C, triethyl orthoformate (4 mL) was added dropwise. The reaction was stirred at 0 °C for 10 min and at room temperature for 10 min. The reaction mixture was poured into cold water (200 mL) and the solid collected by filtration. The solid was washed with a solution of methanol (10 mL), water (150 mL) and concentrated ammonium hydroxide (10 mL) and gave after drying and chromatography on neutral alumina using CH_2Cl_2/MeOH as eluent 2.42 g of the title compound.

8-Acetyl-3,13,17-tris[2-(methoxycarbonyl)ethyl]-2,7,12,18-tetramethyl-(21*H*,23*H*)-(21,23,24-^{15}N)porphyrin (VII). The monoiminium salt **16** was prepared in the same manner as the unlabeled analogue.[48] The aldehyde **18** (600 mg) and the iminium salt **16** (800 mg) were dissolved in anhydrous methanol (20 mL) at 0 °C, and trifluoroacetic acid (6 mL) was added dropwise. The reaction mixture was stirred at 0 °C for 2 h in the dark and was then poured into a refluxing solution of methanol (500 mL), glacial acetic acid (400 mL) containing copper(II) acetate (8 g), and anhydrous sodium acetate (4 g). The reaction was kept in the dark and refluxed overnight. Subsequent workup, demetalization with cold concentrated sulfuric acid, reesterification with 5% methanolic sulfuric acid, and chromatography on silica gel column gave 177 mg (15%) of the labeled porphyrin free base **VII**.

NMR Measurements. The sealed NMR samples of ACP in CD_2Cl_2 were prepared on a vacuum line as previously described.[23,34] The NMR samples were not flame-sealed as usual, as this procedure produces acid impurities which catalyze the intermolecular proton transfer between ACP molecules even when the frozen solution was kept at 77 K. We, therefore, employed 5-mm NMR tubes attached to a symmetric teflon needle valve. A version was developed where the valve (10 mm o.d.) is placed inside the sample rotor enabling NMR spectra in very pure acid-free CD_2Cl_2 solutions to be measured. This procedure has also the advantage that the sample gas phase does not reach into the rotor region. This prevents reflux of the solvent at elevated temperatures and allows NMR measurements above the solvent boiling point.[34] The NMR spectra were recorded on FT-NMR spectrometers Bruker CXP 100 and MSL 300 working at 90.02 and 300.13 MHz. Sample temperatures were calibrated before and after the NMR measurements with a Pt 100 resistance thermometer (Degussa) embedded in a NMR tube with an estimated accuracy of ±0.5 °C. The spectra were transferred from the NMR computer (Bruker Aspect) to a personal computer and then to the UNIVAC 1108 computer at the Central Computer Center of the University of Freiburg.

NMR Lineshape Analysis. In order to obtain kinetic data by NMR lineshape analysis, it is necessary to set up the appropriate complex matrix M and the corresponding population vector **P** for the exchange problem studied. The calculation of the lineshape from M and **P** is straightforward.[51]

Since the cis tautomers in Figure 1 are not directly observable, the tautomerism of porphyrins such as ACP constitutes a reaction network involving four states: r = 1 ≡ AC, 2 ≡ BD, 3 ≡ CA, 4 ≡ DB. Generally, a nuclear spin is characterized in the state r by the Larmor frequency ν_r. In the absence of high order scalar spin–spin coupling, the NMR lineshape of this nucleus is then characterized by:

$$M = \begin{bmatrix} -k_{12}-k_{14}-\pi W_0+2\pi i\nu_1 & k_{21} & 0 & k_{41} \\ k_{12} & -k_{21}-k_{23}-\pi W_0+2\pi i\nu_2 & k_{32} & 0 \\ 0 & k_{23} & -k_{23}-k_{34}-\pi W_0+2\pi i\nu_3 & k_{43} \\ k_{14} & 0 & k_{34} & -k_{41}-k_{43}-\pi W_0+2\pi i\nu_4 \end{bmatrix} \quad (1)$$

$\mathbf{P} = (p_1, p_2, p_3, p_4)$, 1 ≡ AC, 2 ≡ BD, 3 ≡ CA, 4 ≡ DB,

$$K_{rs} = p_s/p_r = k_{rs}/k_{sr}$$

where K_{rs} is the equilibrium constant of the step r to s. The rate constants in eq 1 depend on the type of isotopic reaction monitored.

The HH and the DD reaction in ACP are monitored in this study by ^{13}C NMR spectroscopy at deuterium fractions $D = 0$ and $\simeq 1$. States 2 (BD) and 4 (DB) are then equivalent. For the lineshape of a remote uncoupled single ^{13}C spin with

$$\nu_1 = \nu_3, \nu_2 = \nu_4 \quad (2)$$

the 4 × 4 matrix expressed in eq 1 reduces to the following two-state problem:

$$M = \begin{bmatrix} -k_{12}-k_{14}-\pi W_0+2\pi i\nu_1 & k_{21}+k_{41} \\ k_{12}+k_{14} & -k_{21}-k_{41}-\pi W_0+2\pi i\nu_1 \end{bmatrix}$$

$$\mathbf{P} = (p_1, p_2) \quad (3)$$

The situation is more complex in the presence of two scalar-coupled ^{13}C spins i and j which form an AB spin system. Writing the chemical shift of spin i in state r as ν_{ri} and the coupling constant of spins i and j in state r as J_{rij}, we can expand eq 3 according to Binsch[51] into

$$M = \begin{bmatrix} -k_{12}-k_{14}-\pi W_0+2\pi i\nu_{1i}\pm i\pi J_{1ij} & k_{21}+k_{41} & \mp i\pi J_{1ij} & 0 \\ k_{12}+k_{14} & -k_{21}-k_{41}-\pi W_0+2\pi i\nu_{2i}\pm i\pi J_{2ij} & 0 & \mp i\pi J_{2ij} \\ \mp i\pi J_{1ij} & 0 & -k_{12}-k_{14}-\pi W_0+2\pi i\nu_{1j}\pm i\pi J_{1ij} & k_{21}+k_{41} \\ 0 & \pm i\pi J_{2ij} & k_{12}+k_{14} & -k_{21}-k_{41}-\pi W_0+2\pi i\nu_{2j}\pm i\pi J_{2ij} \end{bmatrix}$$

$$\mathbf{P} = (p_1, p_2, p_3 = p_1, p_4 = p_2) \quad (4)$$

Eqs 3 and 4 show that only the sum $k_{12} + k_{14}$ can be obtained by ^{13}C lineshape analysis.

(51) Binsch, G. *J. Am. Chem. Soc.* **1969**, *91*, 1304.

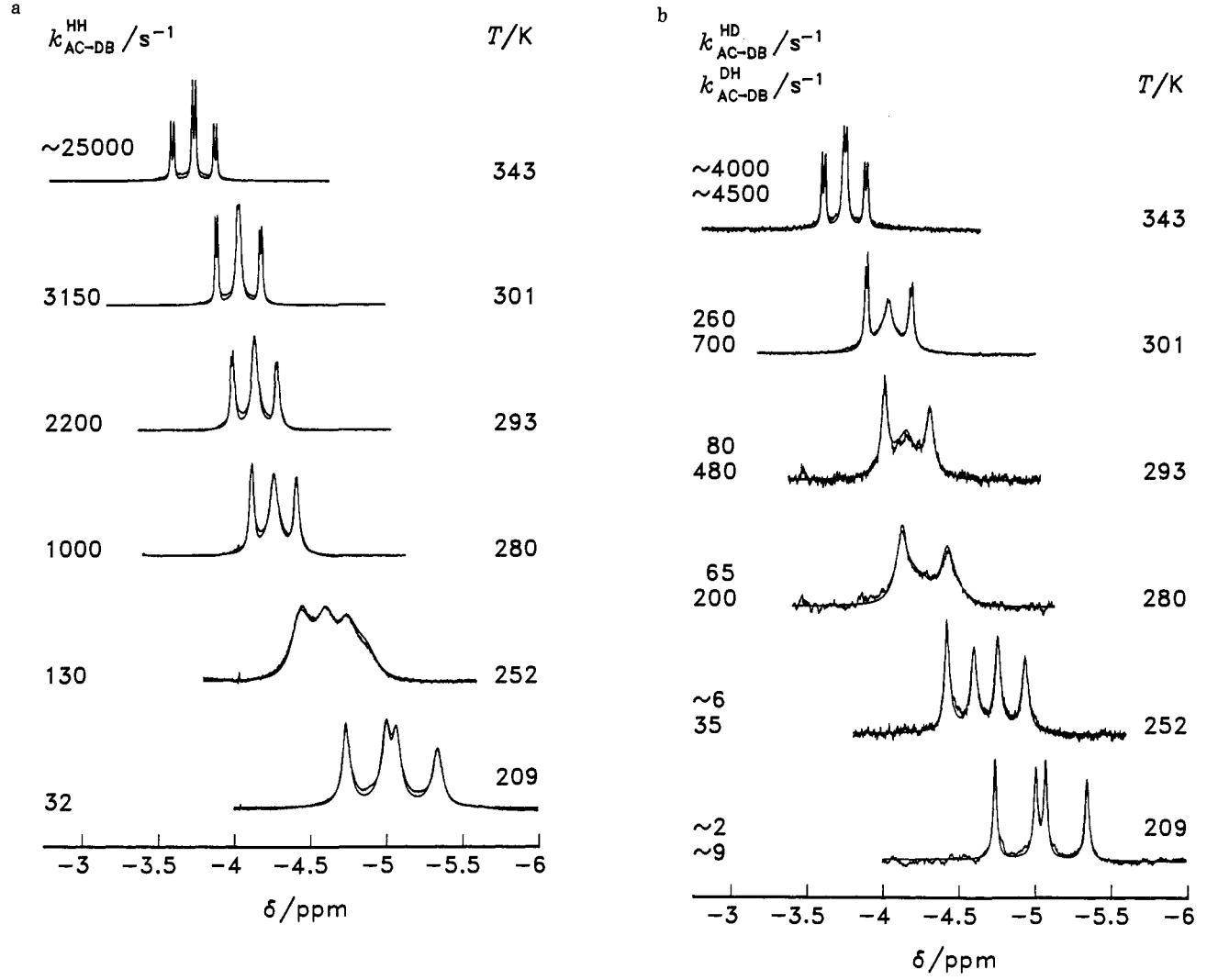

Figure 6. Superposed experimental and calculated 300-MHz ^{1}H NMR signals of the inner protons of ($^{15}N_3$)-ACP in highly purified CD_2Cl_2 (~20 mmol/L) as a function of temperature T. (a) Deuterium fraction $D = 0$; (b) $D = 0.95$. 3-μs $\pi/2$ pulses, 6-kHz spectral width, 3.5-s repetition rate, 2000 scans on average.

Further kinetic information can be obtained by ^{1}H NMR lineshape analyses of the mobile proton signals of ^{15}N-substituted ACP. In this case the Larmor frequencies ν_r in eq 1 have to be replaced by the quantities $\nu_r \pm J_r$, where ν_r is now the chemical shift of a mobile proton in state r and J_r the corresponding coupling constant of the mobile proton with the ^{15}N nucleus to which it is bound. For porphyrins it has been observed that to a good approximation all $J_r = J_{^1H-^{15}N} = J$ are equal. Furthermore, the effective coupling constant of a proton bound to a ^{14}N nucleus is 0 because of the fast quadrupole relaxation of the latter. For a porphyrin triply labeled with the ^{15}N isotope in sites 1, 3 and 4, it follows then that

$$M = \begin{bmatrix} -k_{12}-k_{14}-\pi W_0 + 2\pi i(\nu_1 \pm J) & k_{21} & 0 & k_{41} \\ k_{12} & k_{21}-k_{23}-\pi W_0 + 2\pi i\nu_2 & k_{32} & 0 \\ 0 & k_{23} & -k_{23}-k_{34}-\pi W_0 + 2\pi i(\nu_3 \pm J) & k_{43} \\ k_{14} & 0 & k_{34} & k_{41}-k_{43}-\pi W_0 + 2\pi i(\nu_4 \pm J) \end{bmatrix}$$

$$\mathbf{P} = (p_1, p_2, p_3 = p_1, p_4 = p_2) \tag{5}$$

One pecularity of eq 5 in the fast-exchange range is that only one multiplet is observed where the effective coupling constants are given by

$$J_r^{eff} = p_r J_{^1H-^{15}N} \tag{6}$$

Results

In this section we report the results of our ^{1}H and ^{13}C NMR studies of doubly ^{13}C labeled ACP **I** to **VI** and triply labeled ACP **VII** dissolved in CD_2Cl_2. For the nomenclature see Figures 2–5. First, we will describe the various spectra. From these spectra the equilibrium constants of tautomerism are obtained in a straightforward way. In a subsequent section we will describe how the rate constants were obtained by NMR lineshape analysis.

Description of the Exchange-Broadened ^{1}H NMR Spectra of ACP. Figure 6 shows the superposed experimental and calculated NMR lineshapes of the inner mobile proton signals of triply ^{15}N-labeled ACP, **VII** (see Figure 2), dissolved in CD_2Cl_2 at two deuterium fractions $D = 0$ and $D = 0.95$ as a function of temperature. The calculations are described in a subsequent section. At $D = 0$ the signals stem from the species **VII** ≡ **VII-HH** and at $D = 0.95$ mostly from **VII-HD**. As already reported in our preliminary communication,[34] at low temperature two ^{1}H–^{15}N doublets with equal coupling constants $^1J_{^1H-^{15}N}$ are observed. Therefore, the mobile protons are not located on the nonlabeled nitrogen atom site 22*N* because in this case, a singlet should have been observed in the case of fast ^{14}N relaxation. Since the cis tautomers of porphyrins have a higher energy and are, therefore, not observed, this result indicates that the low temperature doublets in Figure 6 arise from proton sites 21*H* and 23*H*, in other words, from the tautomers AC and CA. As the temperature

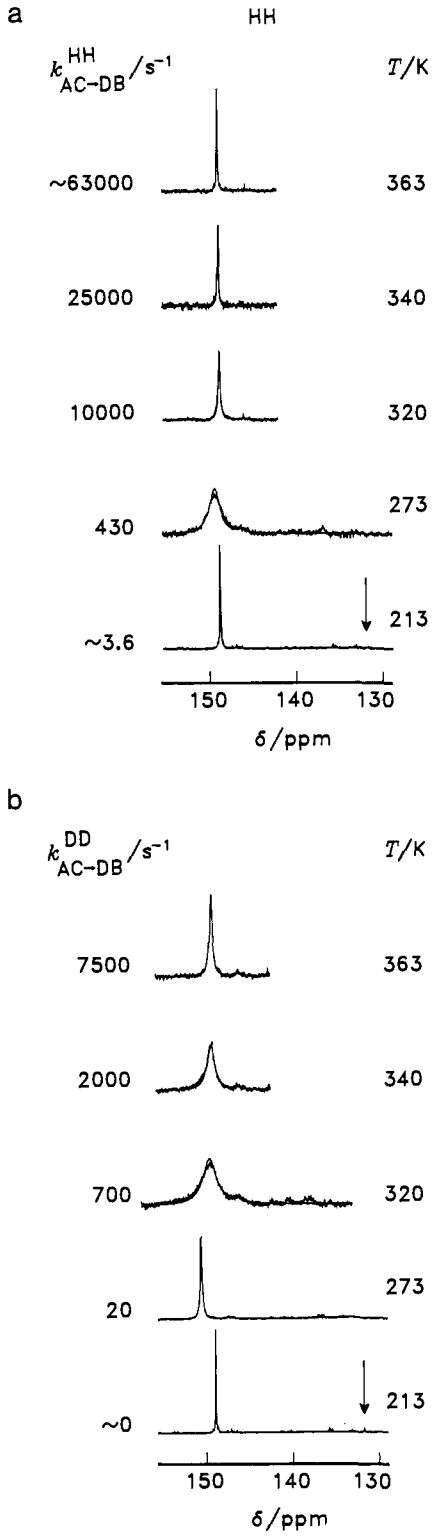

Figure 7. Superposed experimental and calculated ^{13}C NMR signals of the carbon atom C-6 of ($^{13}C_2$)-ACP in CD_2Cl_2 (~20 mmol/L) as a function of temperature T. (a) Deuterium fraction fraction $D = 0$; (b) $D = 0.99$. Experimental conditions: 75 MHz, 3-μs $\pi/2$ pulses, 13-kHz spectral width, 3.5-s repetition rate, 5000 scans on average. The arrow ↓ indicates the tautomers DB and BD visible in the case of slow exchange.

is increased, line broadening and coalescence to a sharp triplets are observed whose components are further split into doublets, due to fast intramolecular proton transfer. Intermolecular proton transfer would lead to a breakdown of the ^1H–^{15}N multiplet. The doublet splitting indicates that at high temperatures the inner protons are also located to a certain fraction in the ^{15}N-labeled

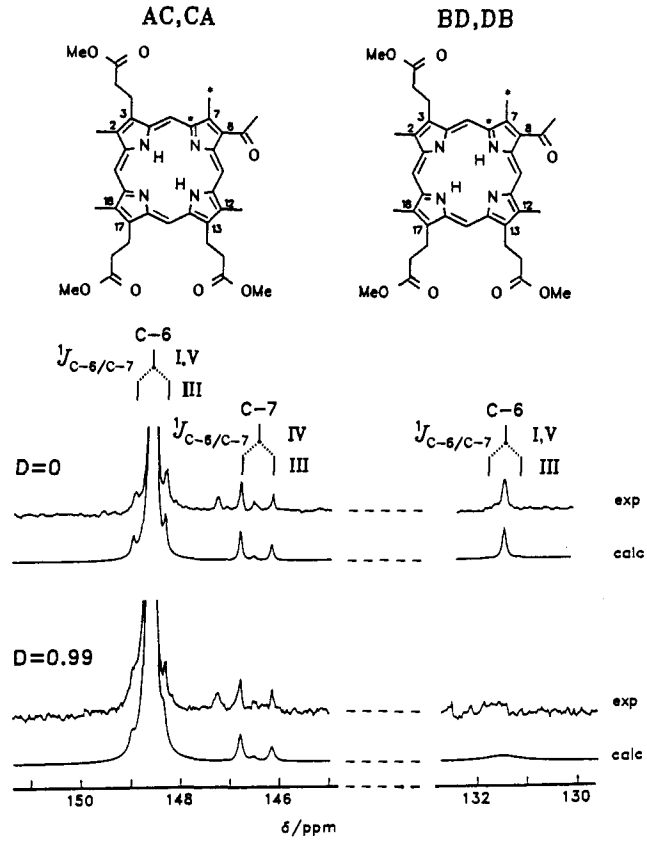

Figure 8. Experimental and calculated ^{13}C NMR spectra of ($^{13}C_2$)-ACP at 213 K with the directly visible 6C signal of the tautomers DB ≡ BD at $D = 0$ and $D = 0.99$. $^1J_{6C/7C}$: ^{13}C coupling constant of the carbon atoms 6 and 7 with $J = 52$ Hz. The bold Roman numbers refer to the isotopomers listed in Figure 4.

nitrogen site 24*N* and in the nonlabeled site 22*N*. In other words, the nondominant tautomers BD and DB must be significantly populated. According to eq 6, the effective doublet splittings are given by $J^{eff}_{24H24N} = p_{BD}J_{^1H-^{15}N} = p_{DB}J_{^1H-^{15}N}$ and the triplet splittings are given by $J^{eff}_{21H21N} = J^{eff}_{23H23N} = p_{AC}J_{^1H-^{15}N} = p_{CA}J_{^1H-^{15}N}$. The ratio of the two splittings is thus equal to the equilibrium constant K of the tautomerism

$$K = (p_{BD} + p_{DB})/(p_{AC} + p_{CA}) = p_{DB}/p_{AC} \qquad (7)$$

K increases with temperature as can be observed in the top spectra of Figure 6. The averaged line position is given by

$$\nu_{av} = (\nu_1 + K\nu_2 + \nu_3 + K\nu_4)/2(1 + K) \qquad (8)$$

Note that the temperature where the exchange-broadened doublets coalesce into an exchange-broadened triplet is higher in the HD case as compared to the HH case. This effect arises from a significant kinetic HH/HD isotope effect. Note also that the signals shift monotonously to higher field as temperature is lowered. This shift arises from the aggregation of ACP at low temperatures.

Description of the Exchange-Broadened ^{13}C NMR Spectra of ACP. Unfortunately, it was not possible to detect the tautomers BD and DB directly by ^1H NMR in the slow-exchange region; however, we succeeded by ^{13}C NMR of ^{13}C-labeled ACP. The dominant species is **I** (for the nomenclature see Figures 2 and 4) which contains two ^{13}C labels in the 6*C* position and the methyl group located on 7*C*. Spectra were taken at $D = 0$ and $D = 0.99$ and are shown in Figures 7 and 8. The signals at $D = 0$ stem mainly from **I-HH** and those at $D = 0.99$ from **I-DD**. Only the region of the ring carbon atoms is shown.

Let us first discuss the low temperature spectra at 213 K which are expanded in Figure 8. A small expected scalar coupling between the methyl carbon and 6*C* in **I** is not resolved. Therefore,

carbon atom 6*C* of the main tautomer of **I** contributes a strong singlet at 148.7 ppm to the spectra. Species **V** (Figure 4) also contributes to this signal. As shown in Figure 8, the singlet is accompanied by two small sidebands of unequal intensity. These sidebands are easily assigned to the low-field doublet of an AB spin system, the high-field doublet appearing at 146.6 ppm. This AB spin system must arise from the carbon atoms 6*C* and 7*C* of **III**. We measured a coupling constant of J_{6C7C} = 52 Hz. The signal of 7*C* appears at the higher field and contains a small singlet inside which stems from 7*C* of species **IV**. The small signal at 147.3 ppm stems from a ^{13}C atom in natural abundance and was not further assigned. By lineshape analysis, it was possible to obtain rough estimates of the relative contributions of the various ^{13}C-labeled ACP species. We obtained ratios of 1:6:100 for species **IV**/**III**/**I** + **V**. These values are not corrected for different relaxation dynamics and nuclear Overhauser effects.

Of special interest is a weak singlet at 131.5 ppm characterized in Figure 7 by arrows which shows exchange broadening at D = 0 but which is sharp at D = 0.99. This signal disappears at higher temperatures. We, therefore, assign this signal to the 6*C* carbon atom of the nondominant tautomers BD and DB of **I**. Assuming that relaxation dynamics and nuclear Overhauser effects are the same in both environments, we can estimate the ratio of the two tautomers by lineshape simulation.

Let us now discuss how the ^{13}C NMR spectra change when the temperature is increased. As mentioned above, the 6*C* signal of the nondominant tautomers BD and DB broadens rapidly and disappears as temperature is raised. The 6*C* signal of AC and CA also broadens and sharpens again at higher temperatures as demonstrated in Figure 7. Note that the temperature, where the maximum line broadening is observed, rises significantly when ACP is deuterated in the mobile proton sites. This effect arises from a kinetic HH/DD isotope effect. As in the case of ^{1}H–^{15}N signals in Figure 6, the 6*C* signals of ACP also shift to lower field as temperature is increased; however, at higher temperatures the signal seems to be independent of temperature. This effect can be understood as follows. At high temperature there is only one coalesced 6*C* signal whose frequency is given by

$$\nu_{av} = p_{AC}\nu_{AC} + p_{CA}\nu_{CA} + p_{BD}\nu_{BD} + p_{DB}\nu_{DB} = \frac{1}{1+K}\nu_{AC} + \frac{K}{1+K}\nu_{BD} \quad (9)$$

because $\nu_{AC} = \nu_{CA}$ and $\nu_{BD} = \nu_{DB}$. Since $\nu_{AC} > \nu_{BD}$, the average signal should shift to higher field when the temperature is increased because of the increase in K. Since ν_{AC} and ν_{BD} shift to lower field, both shifts compensate in the fast-exchange region. Note, however, that the difference in the chemical shifts $\Delta\nu = \nu_{AC} - \nu_{BD}$ was not affected by temperature changes within the margin of error. This result was verified at D = 0.99 where it was possible to measure $\Delta\nu$ in the slow-exchange region and by lineshape analysis as described below.

Evaluation of the Thermodynamic and Kinetic Data by Lineshape Analysis. Thermodynamics of the ACP Tautomerism. The first parameters which had to be established were the equilibrium constants K of the tautomerism as a function of temperature. As shown in the previous paragraph, the K values could be obtained at high temperatures by ^{1}H NMR from the effective coupling constants and at low temperature by ^{13}C NMR from the intensity ratio of the tautomers at D = 0.99. In order to increase the precision of the results these parameters were obtained by lineshape analysis. The results are assembled together with other static and kinetic parameters in Table I.

A van't Hoff plot of all log K values vs $1/T$ revealed a good agreement between the data obtained by ^{1}H and ^{13}C NMR as shown in Figure 9. The dependence of the equilibrium constants with temperature can be expressed by the equation

Table I. Results of the NMR Lineshape Analyses of the ^{13}C NMR Spectra of ^{13}C-Labeled ACP Dissolved in CD_2Cl_2

T, K	k^{HH}, s^{-1a}	k^{DD}, s^{-1}	K^b	D	$\Delta\nu$, Hz	W_0, Hz
213	~3.6	–	0.043[e]	0.99	1297[c]	5.0
245	55	–	0.065[f]	0.99	1300[c]	5.0
273	430[g]	20	0.087[f]	0.99	1302[c]	6.0
305	7500[g]	250	0.115[f]	0.99	1300[d]	6.5
320	10000[g]	700	0.128[f]	0.99	1300[d]	6.0
340	25000[g]	2000	0.145[f]	0.99	1300[d]	6.0
363	63000[g]	7500	0.165[f]	0.99	1300[d]	5.5
380	–	15000	0.180[f]	0.99	1300[d]	6.0

[a] $k^{LL} = k^{LL}_{AC\rightarrow DB}$, LL = HH or DD. [b] K: equilibrium constant of the tautomerism AC ⇌ DB. [c] $\Delta\nu$ chemical shift difference of the carbon atoms 6C in the two tautomers obtained by simulation of the spectra at D = 0.99. [d] $\Delta\nu$: obtained by simulation of the spectra at D = 0 using the known value of k^{HH}. [e] Value directly observed from the spectra at a deuterium fraction of D = 0.99. [f] Calculated according to eq 10. [g] Calculated using eq 14.

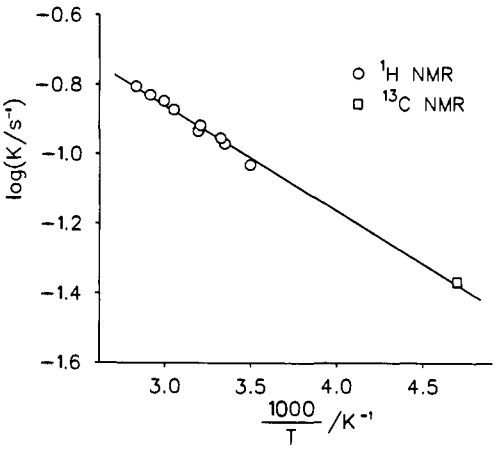

Figure 9. Van't Hoff plot of the equilibrium constant K of tautomerism defined in eq 6. The solid line corresponds to eq 9.

$$K = 1.14 \times \exp(-5.82\ \text{kJ mol}^{-1}/RT) \quad (10)$$

The reaction entropy is, therefore, very close to 0. Additionally, in view of the fact that the high-temperature data stem from measurements at D = 0 and the low-temperature data from measurements at D = 0.99, it seems that within the margin of error there is no equilibrium isotope effect on the tautomerism of ACP.

NMR Lineshape Analysis of ACP. By a combination of ^{1}H NMR and ^{13}C NMR lineshape analysis at different deuterium fractions of the inner proton sites of ACP it was possible to obtain the rate constants and kinetic isotope effects of the ACP tautomerism. For convenience, we express the observed rate constants of the individual isotopic reactions in the form

$$k_{ML_1NL_2\rightarrow XL_1YL_2} = k^{L_1L_2}_{MN\rightarrow XY} \quad (11)$$

characterizing the jump of the light isotope L_1 from ring M to ring X and of L_2 from ring N to ring Y.

In order to facilitate the analysis of the spectra, care was taken to measure samples with different deuterium fractions D in the inner proton sites under the same conditions, i.e. concentration of ACP and temperature as already noted in our previous publication.[34] All parameters of the lineshape simulations are assembled in Tables I and II.

Let us first discuss the lineshape of the ^{1}H NMR signals of the inner protons of **VII**-HH shown in Figure 6. The NMR lineshape theory for the simulation of these signals is given by eq 5. The first problem to be solved was to decide whether the rings A and C in ACP are equivalent in good approximation. In this case, the following equation should hold, as can be inferred from Figure 1:

$$k_{12} \equiv k^{LL}_{AC\rightarrow BD} = k_{14} \equiv k^{LL}_{AC\rightarrow DB},\ \text{LL} = \text{HH, DD} \quad (12)$$

Table II. Static and dynamic Parameter of the ^1H NMR Experiments Performed at 90 and 300 MHz on $^{15}N_3$-labeled ACP Dissolved at ~38 and ~12 mmol/L in CD_2Cl_2[a]

T, K	ν_1, Hz	ν_2, Hz	ν_3, Hz	ν_4, Hz	k^{HH}, s^{-1}	k^{HD}, s^{-1}	k^{DH}, s^{-1}	K[b]	D	W_0, Hz	J, Hz
179.9	−573.0[c]	−503.0[e]	−638.0[c]	−573.0[e]	–	–	–	0.023[d]	0	14.0	100.6
210.1	−519.0[c]	−450.0[e]	−570.0[c]	−519.0[e]	~5	–	–	0.041[d]	0	10.0	100.4
223.0	−496.0[c]	−446.0[e]	−540.0[c]	−496.0[e]	~13	–	–	0.049[d]	0	8.0	100.4
234.2	−479.0[c]	−389.0[f]	−518.0[c]	−479.0[f]	45	–	–	0.057[d]	0	4.5	100.3
252.0	−460.0[e]	−350.0[f]	−489.0[e]	−460.0[f]	135	–	–	0.071[d]	0	6.3	98.4
262.1	−446.0[e]	−356.0[f]	−472.0[e]	−446.0[f]	300	–	–	0.079[d]	0	5.0	98.6
266.1	−441.0[e]	−350.0[f]	−464.5[e]	−441.0[f]	420	–	–	0.082[d]	0	5.2	98.0
274.4	−430.6[e]	−371.0[f]	−449.2[e]	−430.6[f]	750	–	–	0.089[d]	0	6.0	97.2
286.4	−418.5[e]	−368.0[e]	−432.7[e]	−418.5[e]	1700	–	–	0.093[c]	0	5.0	97.7
298.9	−406.5[e]	−316.5[e]	−420.5[e]	−406.5[e]	6750	–	–	0.107[c]	0	5.0	97.6
313.1	−393.3[e]	−305.5[e]	−405.1[e]	−393.3[e]	7000	–	–	0.116[c]	0	6.0	97.5
333.7	−375.9[e]	−281.0[e]	−389.5[e]	−375.9[e]	~25000	–	–	0.142[c]	0	3.7	97.7
353.0	−360.5[e]	−318.5[e]	−370.5[e]	−360.5[e]	~50000	–	–	0.157[c]	0	6.0	97.5
229.9	−1472[c]	−1100[e]	−1553[c]	−1472[e]	32	–	–	0.054[d]	0/0.95	4.3	101.0
252.1	−1377[c]	−1000[e]	−1431[c]	−1377[e]	130	~6	35	0.071[d]	0/0.95	3.7	100.0
265.8	−1327[c]	−950[f]	−1365[c]	−1377[f]	420	12	80	0.082[d]	0/0.95	2.1	99.5
273.9	−1296[e]	−925[f]	−1331[e]	−1296[f]	650	35	130	0.089[d]	0/0.95	1.9	99.0
280.4	−1282[e]	−900[f]	−1312[e]	−1292[f]	1000	65	200	0.094[d]	0/0.95	1.8	98.0
286.3	−1264[e]	−885[c]	−1293[e]	−1264[f]	1600	70	290	0.099[d]	0/0.95	1.7	97.7
292.9	−1253[e]	−873[e]	−1273[e]	−1253[e]	2200	80	480	0.105[d]	0/0.95	1.6	97.7
301.0	−1220[e]	−830[e]	−1240[e]	−1220[e]	3150	260	700	0.111[c]	0/0.95	1.6	97.4
311.6	−1201[e]	−830[e]	−1211[e]	−1201[e]	5500	450	1450	0.121[c]	0/0.95	1.7	97.0
327.4	−1170[e]	−800[e]	−1176[e]	−1170[e]	12000	~1600	~2000	0.134[c]	0/0.95	2.2	97.0
342.9	−1144[e]	−770[e]	−1148[e]	−1144[e]	25000	~4000	~4500	0.148[c]	0/0.95	2.7	96.7

[a] $k^{LL} \equiv k^{LL}_{AC\rightarrow DB}$, LL = HH, HD or DD. [b] K: Equilibrium constant of the tautomerism AC⇌DB. [c] Evaluated without any assumptions. [d] Calculated according to eq 10. [e] Extrapolated according to eq 8. [f] Parameters obtained by nonlinear least squares fitting of the calculated to the experimental lineshapes. In the lineshape simulations at $D = 0.95$ the presence of 5% of HH species was taken into account.

Note that for the tautomerism of some 2-substituted porphyrins, it was found that $k^{HH}_{AC\rightarrow BD} \neq k^{HH}_{AC\rightarrow DB}$.[33] As previously,[34] we obtain a perfect fit of the lineshapes of **VII-HH** assuming the validity of eq 12, as shown in Figure 6. In order to calculate the spectra, it was necessary to know the values of the populations p_i, the linewidths in the absence of exchange W_0, and the chemical shifts ν_1. As discussed above, the values of p_i could be taken from eq 10. In the slow-exchange region between 180 and 240 K the value of W_0 could be taken from the spectra at $D = 0.85$ where the signals of the inner proton are not affected by the exchange due to the large kinetic isotope effect. Since molecular motions of ACP are independent of the deuterium fraction of the inner proton sites all line-broadening due to slow molecular tumbling[10-12] was eliminated in this way. In the fast-exchange range, W_0 could be obtained from the outer signal components. In the intermediate range, the W_0 values were extrapolated. A more serious problem which required special attention was the determination of the chemical shifts ν_r which depend on temperature and concentration in a nonlinear way because of molecular aggregation. Below 260 K the values of ν_1 and ν_3 could be obtained directly from the spectra at $D = 0.85$ where line-broadening is much smaller as demonstrated in Figure 6, parts a and b. ν_1 was assigned to 21*H* and the proton on ring A and ν_3 to 23*H*. Note that this assignment is not unique and could be reverse. However, the symmetry properties of eq 5 are such that this inversion does not affect the lineshapes, i.e. the kinetic results. The chemical shift ν_2 of the proton on ring B in tautomer 2, i.e. of 22*H* was found to strongly induce an asymmetry of the low-temperature lineshapes in Figure 6, parts a and b. The degree of this asymmetry depends in a unique way on ν_2. Therefore, ν_2 could be evaluated by lineshape analysis in the slow-exchange range. Similarly, it was found that the chemical shift ν_4 of the proton on ring D in tautomer 2 is close to ν_1 and ν_3. This is not surprising in view of the similar structure of the pyrrole rings A, C, and D by contrast to B. A good fit was obtained by setting $\nu_1 = \nu_4$. In the intermediate temperature range the values of ν_r were extrapolated from low temperature assuming a similar temperature dependence of all line positions which could be taken from the position of the averaged signal. Small uncertainties of the ν_r values did not lead to systematic errors in the lineshape analysis of the spectra at higher temperatures, e.g. at 301 K where the lineshapes are almost independent on the various chemical shifts. In this range the rate constants could be obtained without assumptions from the differential line-broadening of the inner and the outer lines of the ^1H–^{15}N multiplet.

At $D = 0.85$, the dominant contribution to the ^1H NMR signal of the inner proton sites stems from the species **VII-HD**. As mentioned in the introduction and as can be inferred from Figure 1 the tautomerism of **VII-HD** has to be characterized by two different rate constants

$$k_{12} \equiv k^{HD}_{AC\rightarrow BD} \simeq k^{DH}_{AC\rightarrow DB} \neq k_{14} \equiv k^{HD}_{AC\rightarrow DB} \simeq k^{DH}_{AC\rightarrow BD} \quad (13)$$

In fact, we recognized this result only when we tried to simulate the signal of the HD species: a good fit of the signal could not be achieved when using only one rate constant $k_{12} = k_{14}$ as in the case of **VII-HH**. We did not recognize the validity of eq 13 in our previous ^1H NMR study at 90 MHz[34] because of a low signal-to-noise ratio of the inner proton signals of **VII-HD** and because of the smaller chemical shifts at lower field strength. Therefore, Table II does not contain the rate constants for the latter species published previously.[34]

The effect of varying the rate constants in the fast-exchange range is shown in the theoretical spectra of Figure 10. There are characteristic intensity and line width differences of the various line components of the exchange-broadened multiplet. We are confident that we have good evidence that in the case of ACP-HD $k_{14} = k^{HD}_{AC\rightarrow DB}$ is definitively smaller than $k_{12} = k^{HD}_{AC\rightarrow BD} \simeq k^{DH}_{AC\rightarrow DB}$.

Let us now discuss the lineshape analysis of the ^{13}C spectra of **I-HH** and **I-DD** shown in Figure 7. These experiments were performed in order to obtain the kinetic HH/DD isotope effects on the tautomerismof ACP. The spectra were calculated using eqs 3 and 4. First, we calculated the spectra at $D = 0$. In the slow-exchange range W_0 and the chemical shift difference $\Delta\nu = \nu_1 - \nu_2$ of carbon sites 6*C* in tautomers AC (CA) and in tautomers BD (DB) could be obtained from the spectra at $D = 0.99$, and only the sum of $k_{12} + k_{14} = 2k_{12} = 2k^{HH}_{AC\rightarrow DB}$ was adapted. k_{12} was in good agreement with the values obtained by ^1H NMR. For the simulations of the ^{13}C spectra of $D = 0$ and higher temperatures the k_{12} values known from the ^1H NMR experiments were then used and only $\Delta\nu$ was further adapted. Thus, $\Delta\nu$ could be obtained without assumptions in a large temperature range.

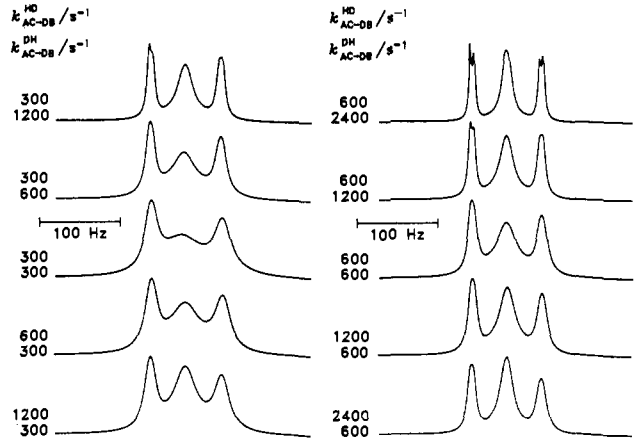

Figure 10. Calculated ^{1}H NMR signals of the inner protons of triply ^{15}N-labeled ACP for different sets of rate constants $k^{HD}_{AC\rightarrow DB}$ and $k^{DH}_{AC\rightarrow DB}$ expected for a temperature range between 300 and 310 K.

We found that $\Delta\nu$ did not change with temperature although the individual values of ν_1 and ν_2 shifted to lower field as the temperature was raised. With the known values of $\Delta\nu$ we were then able to obtain $k^{DD}_{AC\rightarrow DB}$ from the spectra at $D = 0.99$. In the fast-exchange range the values of W_0 were taken from the spectra at $D = 0$. All results are assembled in Table I.

Temperature Dependence of the Rate Constants. The dependence of the rate constants in Tables I and II were evaluated assuming Arrhenius laws. We obtained the following results for the reaction steps in Figure 1:

$$\text{ACP-HH: } k_{12} = k_{14} = k^{HH}_{AC\rightarrow DB} = 10^{10.4\pm0.2}\exp(-40 \pm 1\ \text{kJ mol}^{-1}/RT),\quad 230\ \text{K} \le T \le 327\ \text{K},\ k^{HH}_{AC\rightarrow DB}(298) \simeq 2840\ \text{s}^{-1} \quad (14)$$

$$\text{ACP-HD: } k_{14} = k^{HD}_{AC\rightarrow DB} = 10^{11.3\pm1}\exp(-52 \pm 5\ \text{kJ mol}^{-1}/RT),\ 266\ \text{K} \le T \le 311\ \text{K},\ k^{HD}_{AC\rightarrow DB}(298) \simeq 180\ \text{s}^{-1} \quad (15)$$

$$k_{12} = k^{HD}_{AC\rightarrow BD} = k^{DH}_{AC\rightarrow DB} = 10^{10\pm0.3}\exp(-41 \pm 1.3\ \text{kJ mol}^{-1}/RT),\quad 252\ \text{K} \le T \le 312\ \text{K},\ k^{DH}_{AC\rightarrow DB}(298) \simeq 670\ \text{s}^{-1} \quad (16)$$

$$\text{ACP-DD: } k_{12} = k_{14} = k^{DD}_{AC\rightarrow DB} = 10^{11.5\pm0.2}\exp(-53.5 \pm 0.6\ \text{kJ mol}^{-1}/RT),\quad 273\ \text{K} \le T \le 380\ \text{K},\ k^{DD}_{AC\rightarrow DB}(298) \simeq 150\ \text{s}^{-1} \quad (17)$$

The errors given here are of a pure statistical nature and do not include possible systematic errors. We obtain the following kinetic isotope effects at 298 K:

$$k^{HH}_{AC\rightarrow DB}/k^{HD}_{AC\rightarrow DB} \simeq 16,\ k^{HH}_{AC\rightarrow DB}/k^{DH}_{AC\rightarrow DB} \simeq 4,\quad k^{HH}_{AC\rightarrow DB}/k^{DD}_{AC\rightarrow DB} \simeq 19,\ k^{HD}_{AC\rightarrow DB}/k^{DD}_{AC\rightarrow DB} \simeq 1.2,\quad k^{DH}_{AC\rightarrow DB}/k^{DD}_{AC\rightarrow DB} \simeq 4.5 \quad (18)$$

The complete Arrhenius diagram of the ACP tautomerism is shown in Figure 11.

Discussion

In the previous section we have described the kinetic HH/HD/DH/DD isotope effects of a reversible intramolecular nondegenerate double proton transfer reaction. The molecule studied was ACP whose complete proton transfer pathways are

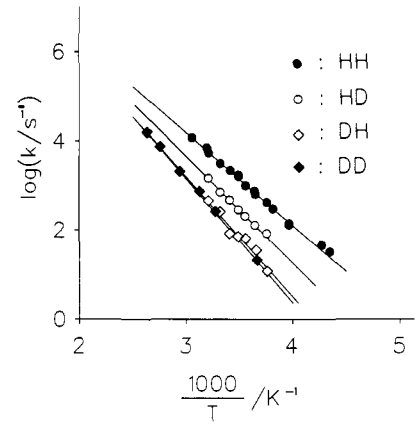

Figure 11. Arrhenius plot of the rate constants $k^{LL}_{AC\rightarrow DB}$ LL = HH, HD, DH, and DD of the tautomerism of ACP dissolved in CD_2Cl_2.

shown in Figure 1. The different tautomers are conveniently characterized by a two-letter combination XY = AC, CA, BD, DB etc. indicating the pyrrole rings to which the inner protons are attached. By triply labeling ACP with the ^{15}N isotope according to Figure 2, it was found that the tautomers AC and CA are the dominant species, whereas tautomers BD and DB are present only to a minor extent. Thermodynamic and kinetic quantities of the tautomerism were obtained from ^{1}H NMR lineshape analysis of the inner proton signals and by ^{13}C NMR lineshape analysis of the signals of the carbon site 6*C* which was enriched with the ^{13}C isotope. We find that the forward rate constants of the HH migration in ACP are surprisingly close to those of symmetric 5,10,15,20-tetraphenylporphyrin[13,14] and only a factor of 2 slower than those of the related quasisymmetric coproporphyrin-III (COPRO)[6,52] which differs from ACP only in the sense that the acetyl group is replaced by a CH_2CH_2-$COOCH_3$ group (Figure 2). For ACP-HH and ACP-DD, tautomers AC and CA as well as tautomers BD and DB are degenerate. However, this degeneracy is in principle lifted in the case of ACP-HD as shown in Figure 1, part b, but within the margin of error of our experiments, no equilibrium hydrogen/deuterium isotope effect was observed; therefore, tautomers AC and CA as well as BD and DB are quasidegenerate in ACP-HD. As a consequence, only one equilibrium constant of tautomerism *K* given by eq 10 is needed in order to describe the thermodynamics of all isotopic reactions in ACP. The reaction enthalpy is 5.8 kJ mol^{-1}; the reaction entropy is close to 0.

In the case of ACP-HH and ACP-DD it was found by lineshape analysis that the rate constants of reaction from tautomer 1 ≡ AC to 2 ≡ BD and from 1 to 4 ≡ DB are equal within the margin of error, i.e. that

$$k_{12} \equiv k^{LL}_{AC\rightarrow BD} \simeq k_{14} \equiv k^{LL}_{AC\rightarrow DB} \text{ for LL = HH, DD} \quad (18)$$

A priori, this result is not trivial in view of the finding that these two quantities differ in other asymmetrically substituted porphyrins.[33] Thus, the transition states of the reaction AC→BD and AC→DB are quasiequivalent when LL = HH and DD. By contrast, the pathways AC→BD and AC→DB are no longer equivalent in the case of ACP-HD where we find that two forward rate constants are needed in order to describe the reaction kinetics. It is a slow process in the case where a deuteron jumps to the acetyl-substituted pyrrole ring B, i.e

$$k_{14} \simeq k_{34} = k^{HD}_{AC\rightarrow DB} < k_{12} \simeq k_{32} = k^{HD}_{AC\rightarrow BD} \simeq k^{DH}_{AC\rightarrow DB} \quad (19)$$

Because of eq 19 we can characterize the ACP tautomerism by the four rate constants $k^{HH}_{AC\rightarrow DB}$, $k^{HD}_{AC\rightarrow DB}$, $k^{DH}_{AC\rightarrow DB}$, $k^{DD}_{AC\rightarrow DB}$ which

(52) Braun, J., Schlabach, M., Limbach, H. H., unpublished results.

all refer to the same step AC→DB. The main part of the following discussion is devoted to the question of how to explain these isotope effects and what information they contain regarding the reaction mechanism.

Interpretation of the Kinetic HH/HD/DH/DD Isotope Effects. Multiple kinetic isotope effects of double proton transfer reactions depend on whether the reaction is concerted or stepwise, whether it is degenerate or non-degenerate, whether it is intra- or intermolecular, and whether tunneling is involved or not. For concerted degenerate double proton transfers in the absence of tunneling, the rule of the geometric mean should hold in good approximation, which states that[13,36,53]

$$k^{HH}/k^{HD} = k^{HD}/k^{DD} \tag{20}$$

This rule should also hold in good approximation for nondegenerate reactions.[36] Tunneling may lead to a breakdown of this rule[13,25,26] but the relation

$$k^{HH} > k^{HD} = k^{DH} > k^{DD} \tag{21}$$

should remain valid.

The multiple kinetic isotope effects of stepwise double proton transfers depend more strongly on the degeneracy of the reaction. In past years, progress has been made especially in the understanding of kinetic HH/HD/DD isotope effects of degenerate intra- and intermolecular double proton transfer reactions.[14,22-26] With regards to these reactions, it was shown that for a stepwise pathway the relation

$$k^{HH} \gg k^{HD} = k^{DH} \cong 2k^{DD} \tag{22}$$

should hold in the absence of secondary isotope effects, even if tunneling is involved. For intramolecular double proton transfers in relatively rigid molecules such as symmetric porphyrins like TPP,[13,14] azophenine,[23] and oxalamidine[24] eq 22 was well fulfilled, i.e. these processes occur stepwise via metastable intermediates. This finding was independently supported in the case of the oxalamidine tautomerism through the observation of strong kinetic solvent effects due to the high polarity of the intermediate and the corresponding transition states.[24]

Recently,[40] the following equations have been derived for the case of a nondegenerate stepwise reversible double proton transfer as the one shown in Figure 1:

$$\frac{k^{HH}_{AC\rightarrow DB}}{k^{DD}_{AC\rightarrow DB}} = SP \tag{23}$$

$$\frac{k^{HH}_{AC\rightarrow DB}}{k^{HD}_{AC\rightarrow DB}} = \frac{S + P\kappa^{HH}}{1 + \kappa^{HH}} \tag{24}$$

$$\frac{k^{HH}_{AC\rightarrow DB}}{k^{DH}_{AC\rightarrow DB}} = \frac{P + S\kappa^{HH}}{1 + \kappa^{HH}} \tag{25}$$

$$\frac{k^{HD}_{AC\rightarrow DB}}{k^{DH}_{AC\rightarrow DB}} = \frac{P + S\kappa^{HH}}{S + P\kappa^{HH}} \tag{26}$$

Here, κ is a commitment factor defined by

$$\kappa = \frac{k^{HH}_{DC\rightarrow AC}}{k^{HH}_{DC\rightarrow DB}} \tag{27}$$

P and S are the primary and secondary kinetic isotope effects of the single proton transfer steps which are assumed to be the same in all reaction steps, i.e.:

(53) Bigeleisen, J. *J. Chem. Phys.* **1955**, *23*, 2264.

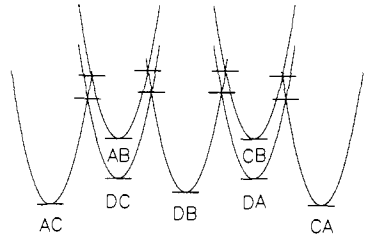

Figure 12. Energy profile (schematically) for the stepwise reaction pathway AC ⇌ CA of the tautomerism of ACP using parabolic potentials.

$$P = \frac{k^{HH}_{AC\rightarrow DC}}{k^{DH}_{AC\rightarrow DC}} = \frac{k^{HD}_{AC\rightarrow DC}}{k^{DD}_{AC\rightarrow DC}} = \frac{k^{HH}_{DC\rightarrow AC}}{k^{DH}_{DC\rightarrow AC}} = \frac{k^{HD}_{DC\rightarrow AC}}{k^{DD}_{DC\rightarrow AC}} \tag{28}$$

$$S = \frac{k^{HH}_{AC\rightarrow DC}}{k^{HD}_{AC\rightarrow DC}} = \frac{k^{DH}_{AC\rightarrow DC}}{k^{DD}_{AC\rightarrow DC}} = \frac{k^{HH}_{DC\rightarrow AC}}{k^{HD}_{DC\rightarrow AC}} = \frac{k^{DH}_{DC\rightarrow AC}}{k^{DD}_{DC\rightarrow AC}} \tag{29}$$

The experimental kinetic HH/HD isotope effects of the tautomerism of *meso*-tetraphenylchlorin could be explained in terms of these equations.[40]

In the following, we discuss whether the kinetic isotope effects on the tautomerism of ACP as expressed by eqs 14–17 can better be explained by either the concerted or the stepwise reaction mechanism.

Concerted Reaction Pathway. In Figure 1, part a the chemical structures of the transition states of the hypothetical concerted reaction pathway are shown for the reaction where one H and one D atom are transferred. There is no reason to believe that the remaining zero-point energies of the H and the D isotopes are much dissimilar in the different transition states. Therefore, $k^{HD}_{AC\rightarrow DB}$, $k^{DH}_{AC\rightarrow BD}$, $k^{HD}_{AC\rightarrow BD}$, and $k^{DH}_{AC\rightarrow DB}$ should all be very much the same and the rule of the geometric mean eq 20 or at least eq 21 should hold in good approximation. The experimental results as expressed by eqs 14–17 do not support this expectation and are therefore not in good agreement with a concerted reaction pathway.

Stepwise Reaction Pathway. The question then arises as to whether the stepwise reaction pathway of Figure 1, part b is in better agreement with the experimental results. In order to discuss this question let us first construct a schematic reaction profile for the stepwise mechanism. This has been done in Figure 12 using the simplest approach with parabolas for the interconversion AC→DB→CA. Since the acetyl-substituted pyrrole ring B in ACP is less basic than the other three rings, all structures with a hydrogen isotope located on this ring have higher energies as compared to the other structures. Therefore, the cis tautomer AB has a higher energy than the cis tautomer DC. This is also the case for BA, BC, and CB which have higher energies than CD, AD, and DA, as well as for the corresponding transition states. Consequently, the exchange AC→DB→CA takes place predominantly via the route AC→DC→DB→DA→CA, whereas the pathway AC→AB→DB→CB→CA does not, to a large extent, contribute to the experimental reaction rates. On the other hand, the exchange AC→BD→CA preferentially proceeds via the pathway AC→AD→BD→CD→CA and only to a minor extent via AC→BC→BD→BA→CA.

The finding expressed by eq 19 that the processes where a D jumps to ring B are slower than the processes where D jumps to another ring leads then to the conclusion that the "left" reaction pathway AC→AD→BD→CD→CA is faster than the "right" reaction pathway AC→DC→DB→DA→CA in the case of ACP-HD. This result can be understood as a stepwise reaction pathway in terms of eqs 23–29. Since the reaction rate constants of ACP-H_2 and symmetric TPP-H_2 are very similar, we assume that P and S are also similar for both substances. Taking the values

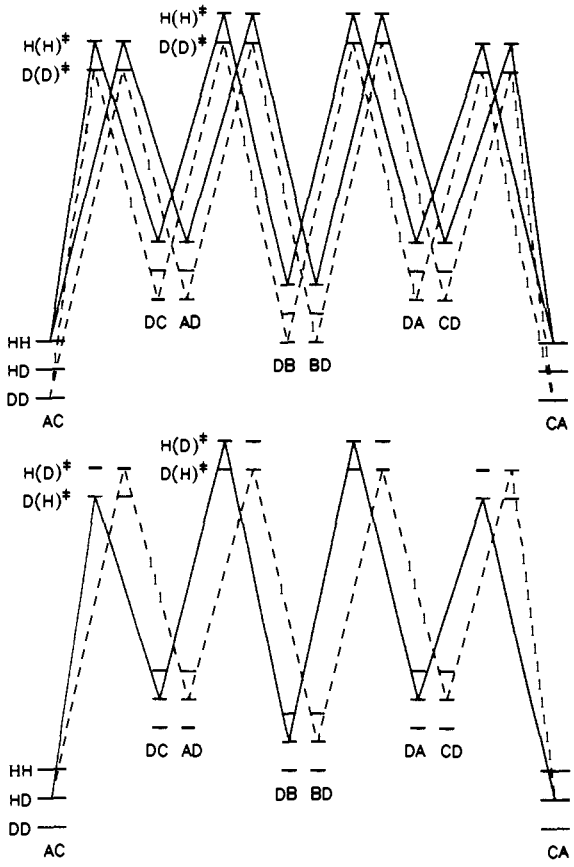

Figure 13. Energy profile for the reaction AC ⇌ CA of ACP. Top: HH, DD reactions. Bottom: HD, DH reactions.

$$P \simeq 0.20 \exp(11.5 \text{ kJ mol}^{-1}/RT),\ P(298) \simeq 20.7 \quad (30)$$

$$S \simeq 1.0 \exp(0.08 \text{ kJ mol}^{-1}/RT),\ S(298) \simeq 1.0 \quad (31)$$

from TPP[14] we can adapt the experimental Arrhenius curves of Figure 11 to eqs 23–29 just by assuming that

$$\kappa \simeq 0.018 \exp(13.4 \text{ kJ mol}^{-1}/RT),\ \kappa(298) \simeq 3.8 \quad (32)$$

The Arrhenius curves calculated by linear regression (eqs 14–18) cannot be distinguished from the curves calculated in this way.

It is interesting to relate these results to those obtained in a recent study of a nondegenerate intermolecular one-sided double proton transfer.[39] In that study a value of $P(298\text{ K}) \simeq 7$ and of $S \simeq 1$ were observed. Whereas the value of S agrees well with the one found here, the value of P is much larger in the reaction studied here. Although caution must be applied when comparing kinetic isotope effects of inter- and intramolecular double proton transfer reactions,[26] the large value of P found here may be ascribed to a substantial tunnel contribution to the ACP tautomerism. It is well known that tunneling plays a role in the tautomerism of porphyrins.[13,14,21] The tunnel contribution is further corroborated by the finding that the preexponential factor of P is substantially smaller than 1 and the difference of the energy of activation is larger than 6 kJ mol^{-1}. Since the factor κ is larger than 1, the backward HH reaction DC→AC is, as expected, slightly faster than the forward reaction DC→DB. In order to clearly demonstrate why the values of $\kappa \neq 1$ lead to the seemingly strange result of $k^{HH}_{AC\rightarrow DB} > k^{DH}_{AC\rightarrow DB} > k^{HD}_{AC\rightarrow DB} \simeq k^{DD}_{AC\rightarrow DB}$ and in order to provide a more comprehensive interpretation of the above results, Figure 13 shows a schematic free energy diagram for the various isotopic reaction pathways. Possible secondary kinetic isotope effects are neglected. In the stable and the metastable states and mobile hydrogen isotopes are bound, leading to three isotopic states labeled in Figure 13 as HH, HD, and DD which are characterized by different zero-point energies. In the transition states, one hydrogen isotope is still "bound" and one isotope is "in flight". The latter is written in parentheses and characterized by a double dagger. If one compares the energetics of the HH and the DD reaction (Figure 13 top) one sees immediately that the DD reaction (dashed lines) requires more energy than the HH reaction (solid lines). The HD and the DH reactions are depicted at the bottom of Figure 13. In the HD reaction (solid line), the proton is in flight in the first step and the deuteron in the second rate-determining step. By contrast, in the DH reaction, the deuteron is transferred in the first step. If κ is large, the energy difference between the two transition states is also large. From eqs 23–27 it follows then that

$$k^{HH}_{AC\rightarrow DB} = k^{DH}_{AC\rightarrow DB} \quad (33)$$

$$k^{HD}_{AC\rightarrow DB} = k^{DD}_{AC\rightarrow DB} = P^{-1}k^{HH}_{AC\rightarrow DB} \quad (34)$$

Since κ is only slightly larger than 1, eq 34 still holds in good approximation but $k^{HH}_{AC\rightarrow DB} > k^{DH}_{AC\rightarrow DB}$. In other words, from the kinetic HH/DH isotope effect the value of κ can be estimated. In Figure 13, κ was set such that the profile of the DH reaction is approximately symmetric.

Conclusions

The synthesis of a ^{13}C and triply ^{15}N-labeled acetylporphyrin ACP (Figure 2) has made it possible to determine the kinetic HH/HD/DH/DD isotope effects of the nondegenerate double hydrogen transfer in this compound by dynamic NMR spectroscopy. The kinetic results can be modeled in a quantitative way in terms of stepwise reaction pathway. No assumptions on whether the hydrogen isotopes tunnel through the barrier or whether they jump over the barrier were necessary in order to come to this conclusion. Rate constants and kinetic isotope effects on the single proton transfer steps were of the same order as in symmetric porphyrins. We find evidence that in the reaction the tautomers AC and CA mainly interconvert via the pathway where one H and one D migrates, AC→AD→BD→CD→CA (Figure 1b), where an H isotope is transferred in both rate-limiting steps AD→BD and BD→CD. Pathway AC→DC→DB→DA→CA is slower because a deuteron is transferred in the rate limiting step of the reaction. In addition, routes involving the intermediates AB, CB, BC and BA do not contribute to the reaction rates.

Acknowledgment. We thank the Deutsche Forschungsgemeinschaft, Bonn-Bad Godesberg, the Fonds der Chemischen Industrie, Frankfurt, and the National Institutes of Health for financial support.